Temperature and pressure induced Raman studies of C_{60} oxide

Trisha Mondal,[1] Ajay Tripathi,[1] Archana Tiwari,[1,a)] Jinying Zhang,[2] Thoudinja Shripathi,[3] and Hisanori Shinohara[4]
[1]*Department of Physics, School of Physical Sciences, Sikkim University, Gangtok 737102, India*
[2]*Center of Nanomaterials for Renewable Energy, State Key Laboratory of Electrical Insulation and Power Equipment, School of Electrical Engineering, Xi'an Jiaotong University, Xi'an 710054, China*
[3]*UGC-DAE CSR, Indore Centre, Khandwa Road, Indore 452001, India*
[4]*Department of Chemistry and Institute for Advanced Research, Nagoya University, Nagoya 464-8602, Japan*

(Received 8 August 2018; accepted 30 October 2018; published online 19 November 2018)

We present temperature, laser power, and pressure dependent Raman spectral analysis of C_{60} oxide ($C_{60}O$) thin films prepared by the photolysis method. The first order temperature, laser power, and pressure coefficients of the Raman frequencies are evaluated and are utilized for evaluating the thermal conductivity of $C_{60}O$. Its thermal conductivity is found to be 0.7 $W\,m^{-1}\,K^{-1}$ which is marginally higher than that of bulk C_{60}. Raman frequencies corresponding to C–O and C–C bonds blue-shift with a decrease in temperature which is attributed to the thermal contraction of $C_{60}O$ molecules. The density functional measurements have been performed to optimize $C_{60}O$ structure. The contraction in the C–O bond length has been corroborated with the experimental Raman shifts at different temperatures and is used to evaluate the linear expansion coefficient of $C_{60}O$. Pressure induced compression and polymerization of $C_{60}O$ clusters are also illustrated. This study highlights the interplay between thermal and mechanical transformations in the $C_{60}O$ cluster which may regulate its thermoelectric properties by tuning the intermolecular interactions. *Published by AIP Publishing.* https://doi.org/10.1063/1.5051396

I. INTRODUCTION

Designing efficient thermoelectric materials for converting heat into electricity is a global challenge. In order to enhance the thermoelectric properties, one may either reduce the thermal conductivity of the material or increase its thermoelectric power.[1,2] As most of the thermoelectric materials are subjected to high temperatures under ambient conditions for their applications, their long term stability is generally desired.

Fullerenes and their derivatives are used in both organic and inorganic nanocomposites to improve their thermoelectric efficiencies.[3–6] Thanks to their ultralow thermal conductivities, the presence of C_{60} in the bulk media limits the phonon transport path which in turn reduces the heat conduction.[7–9] However, it is difficult to maintain pristine C_{60} as it readily reacts with atmospheric oxygen and forms oxide.[10,11]

Two stable oxygen containing fullerene isomers are observed: (i) epoxy like structure (with a single C–C bond) and (ii) annulene like structure (with a broken C–C bond).[12–14] Although there are several reports on the thermal conductivities of empty and endohedral fullerenes, the heat conduction in oxygen containing fullerenes has not been reported to date.[15–17] In oxidized fullerenes, the unpaired electron in $C–O^-$ may contribute to additional electron-phonon interaction which may regulate the thermal conductivity of C_{60} in air.[18]

Raman spectroscopy is often used for understanding the inter- and intra-molecular interactions in fullerenes. The Raman spectra of C_{60} and $C_{60}O$ have been previously reported showing the intermolecular interactions between the cages and the cage functionalization by oxygen. Like C_{60}, most of the cage vibrational modes are present in $C_{60}O$ except that they are split due to the presence of oxygen which lifts the vibrational degeneracy.[19,20] Under thermal and mechanical stress, C_{60} conformation and its interaction with the neighborhood may vary which can affect the heat conduction and thermoelectric efficiency.[21,22]

In this work, we report temperature, laser power, and pressure dependent Raman spectra of $C_{60}O$ film. The first order temperature, laser power and pressure coefficients of the Raman frequencies are evaluated and are utilized to measure the thermal conductivity of $C_{60}O$. Both temperature and pressure influence the structural and optical properties of $C_{60}O$ which modulates its thermal conductivity.

II. EXPERIMENTAL DETAILS

C_{60} was oxidized using photo-oxidation techniques described by Rao *et al.*[23] and Heymann and Chibante.[24] Pristine C_{60} (99.5%, SES Research) dissolved in toluene was simultaneously irradiated with UV light (100 W short arc Hg lamp) and was bubbled with oxygen gas for 3 h. The obtained precipitates were dried in air under ambient conditions for 10 days. The oxidation of C_{60} was confirmed by using the room temperature Raman spectrum which was found to be in accordance with the previous report.[20] The obtained product was kept in CS_2 and was labeled as $C_{60}O$. The solution was drop-casted on a glass substrate, and the prepared thin film (thickness $\sim$ 0.32 mm) was used for the optical measurements.

a)E-mail: archana.tiwari.ox@gmail.com

Temperature dependent Raman characterization of $C_{60}O$ was performed using LABRAM HR-800 spectrometer at an excitation wavelength of 488 nm. The thin-film was mounted in THMS-600 stage, Linkam, UK, where the temperature was varied between 80 K and 300 K in a thermal step of 20 K. In order to avoid the sample heating, 1 mW laser power was imposed on the films during the measurements. After background subtraction and fitting the Raman peaks with Lorentzian profiles, the peak positions were determined.

Laser power dependent Raman measurements were performed at room temperature using the Renishaw inVia RM2000 spectrometer using an excitation wavelength of 514.5 nm. The laser power was varied between 0.1 mW and 0.5 mW. The beam was focused on the sample using 50× objective (numerical aperture, 0.75). In order to evaluate the experimental beam diameter, the image of the focused laser spot on the sample surface was acquired using a calibrated camera mounted on the microscope. The image was analyzed using ImageJ software and its cross-sectional profile is plotted in Fig. 1. The profile is fitted with the Gaussian function where $1/e^2$ width a is found to be 3.6 μm.

High pressure Raman measurements were performed using Diacell Lever Maxi (easyLab) diamond anvil cell equipped with 1 mm diameter culet and stainless steel gasket having 0.25 mm hole. 16:3:1 of methanol–ethanol–water mixture was used as a pressure transmitting medium which maintained the hydrostatic conditions up to 14.5 GPa.[25,26] Raman spectra were obtained using 514.5 nm excitation, where the laser power on the sample was maintained below 3 mW. Ruby chips were loaded in the sample chamber and their luminescence was used to evaluate the pressure.[27]

III. RESULTS AND DISCUSSIONS

A. Temperature dependent Raman analysis

In C_{60}, three Raman peaks at 273, 497, and 1469 cm^{-1} have been assigned to H_g squashing mode, A_g breathing mode, and A_g pentagonal pinch mode, respectively.[28,29] The room temperature Raman spectrum of $C_{60}O$ is shown in Fig. 2. The vibrational modes of $C_{60}O$ are observed in the same characteristic region as that of pristine C_{60}; however, the modes appear split as well as shifted due to the reduced symmetry of C_{60} in the presence of oxygen.[20,28] The Raman spectrum of $C_{60}O$ was acquired in two regions: (i) 200-700 cm^{-1} and (ii) 1000-1600 cm^{-1}. In the lower-frequency region, the appearance of 256.3(3) cm^{-1} and 270.5(1) cm^{-1} peaks in $C_{60}O$ is attributed to the split in the H_g squashing mode of C_{60} where 256.3 cm^{-1} peak arises due to the translation of the bound oxygen atom. The peaks 488.7(2) cm^{-1} and 493.6(1) cm^{-1} in $C_{60}O$ are attributed to the A_g breathing mode of the cage. In the higher-frequency region, the peak at 1458.8(2) cm^{-1} is accompanied by a shoulder peak at 1468.4(2) cm^{-1} which are attributed to photo-polymerization of C_{60}.[23,30] In this work, the thermal analysis is performed on 256.3 cm^{-1}, 270.5 cm^{-1}, 1458.8 cm^{-1}, and 1468.4 cm^{-1} vibrational modes of $C_{60}O$.

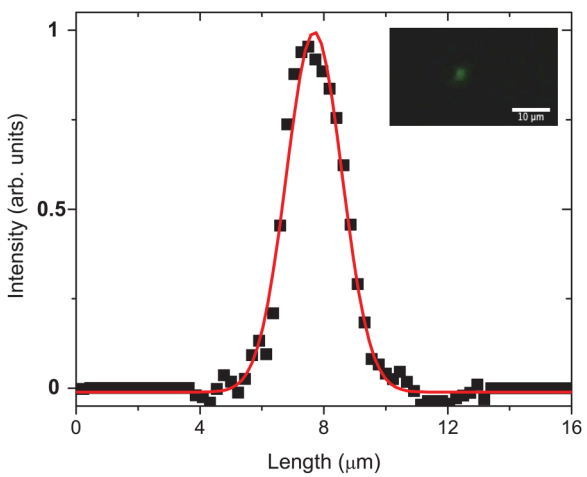

FIG. 1. Profile of the laser spot on the surface of the sample (square) fitted with the Gaussian function (line). The inset shows the image of the laser spot (laserpower = 0.15 mW) acquired using 50× objective on the Raman microscope.

The Raman spectra of $C_{60}O$ in the temperature range 80–300 K are shown in Fig. 2. Upon decreasing the temperature to 80 K, all vibrational modes blueshift. At 80 K, 256.3 cm^{-1} and 270.5 cm^{-1} peaks are observed at 257.3(3) and 271.6(1) cm^{-1}, whereas 1458.8 cm^{-1} and 1468.4 cm^{-1} peaks are seen at 1462.3(1) cm^{-1} and 1471.8(4) cm^{-1}, respectively. The thermal variation of 256.3 cm^{-1}, 270.5 cm^{-1}, 1458.8 cm^{-1}, and 1468.4 cm^{-1} peaks is shown in Fig. 3. The shift in Raman frequencies (ω) with temperature can be related to the following equation:[31]

$$\omega(T) = \omega_0 + \chi_T T, \tag{1}$$

where ω_0 is the frequency at absolute zero and χ_T is the first order temperature coefficient. The thermal variation of 256.3, 270.5, 1458.8, and 1468.4 cm^{-1} peaks is fitted with the above equation (see Fig. 3), and the fitting parameters ω_0 and χ_T are tabulated in Table I.

Negative temperature coefficient χ_T arises due to thermal contraction of the sample which affects both bond lengths and inter- and intra-molecular interactions. χ_T of $C_{60}O$ are found comparable to that of pristine C_{60} revealing that both molecules experience similar contraction with decrease in temperature.[32] However, in the low frequency region, χ_T of $C_{60}O$ and C_{60} is smaller than that of Gd and Dy doped C_{82}.[16] This could be attributed to the rigid skeleton of C_{60} as compared to that of C_{82}. Linewidths of the lower frequency peaks remain nearly constant with the temperature illustrating minimal anharmonic contributions to the Raman shifts.

In order to elucidate the dynamics of C–O bond in $C_{60}O$, the calculations within density functional theory (DFT) are performed on the optimized structure of $C_{60}O$ (annulene-like) by varying the C–O bond length. The theoretical Raman spectrum of a $C_{60}O$ single molecule was obtained by using the functional B3LYP method with an extended 6-31G(d) basis set (optionSCF = Tight). Molecular modeling and vibrational spectral analysis are performed using Gaussian 09.[33] The obtained Raman spectrum is compared with the experimental result in the frequency range of 200-600 cm^{-1} and is shown in Fig. 4(a). The notable peaks

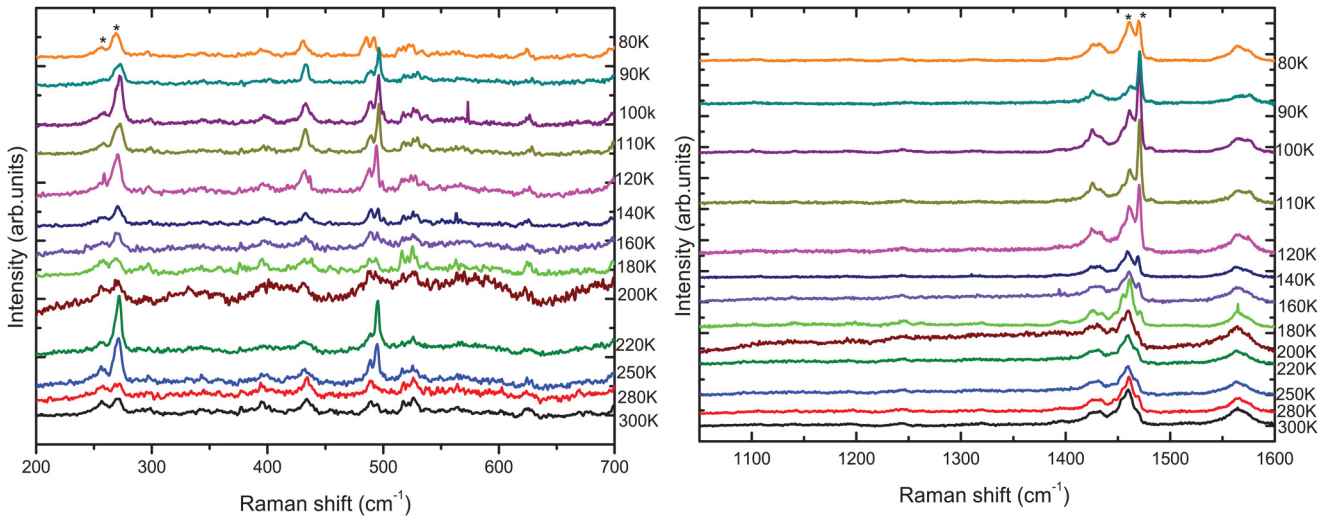

FIG. 2. Temperature dependent Raman spectra of $C_{60}O$ measured between 80 K and 300 K using 488 nm laser excitation. The thermal analysis is performed on the peaks marked by stars.

can be seen at 235.7, 242.6, and 272.9 cm^{-1}, whereas experimentally, the corresponding Raman peaks were observed at 256.3 cm^{-1} and 270.5 cm^{-1}. The experimental spectrum is acquired for $C_{60}O$ films, whereas the DFT measurement is done on a single molecule and, this is why, a small variation in the two results can be noticed.

From the optimized structure of $C_{60}O$, C–O bond length is found to be 1.398 Å which is in line with the previous reports.[34,35] To observe the changes in the Raman frequencies due to contraction, we deliberately changed the C–O bond length by 0.7%. In Fig. 4(b), the observed shift in the 235.7 cm^{-1} peak is shown as a function of C–O bond length and is fitted with an exponential decay function. As C–C bond lengths are constrained to remain unchanged, no shift in the 273 cm^{-1} peak is noticed. Both calculated and experimental results illustrate thermal contraction in C–O bond blueshifts the Raman peak at 235.7 cm^{-1}. Experimentally, the peak at 256.5 cm^{-1} blueshifts by 1 cm^{-1} at 80 K as compared to that at room temperature which is ascribed to thermal contraction in C–O bond by 0.009(2) Å. The linear thermal expansion coefficients of bulk and thin films of C_{60} have been reported previously by Gugenberger *et al.*[36] and Pugachev *et al.*[37] using dilatometry and electron optical techniques, respectively. However, no report on the oxide molecule is found. We evaluated the thermal expansion coefficient of $C_{60}O$ and it was found to be 30×10^{-6} K^{-1} which is slightly larger than that of pristine C_{60} at 80 K ($\sim 20 \times 10^{-6}$ K^{-1}).[36,37] Owing to their reduced symmetry as compared to that of C_{60}, the oxide molecules interact weakly with each other which may lead to increase in their expansivity as compared to the unoxidised ones.

B. Thermal conductivity of $C_{60}O$

Thermal conductivity can be estimated using the first order temperature and laser power coefficients of the Raman

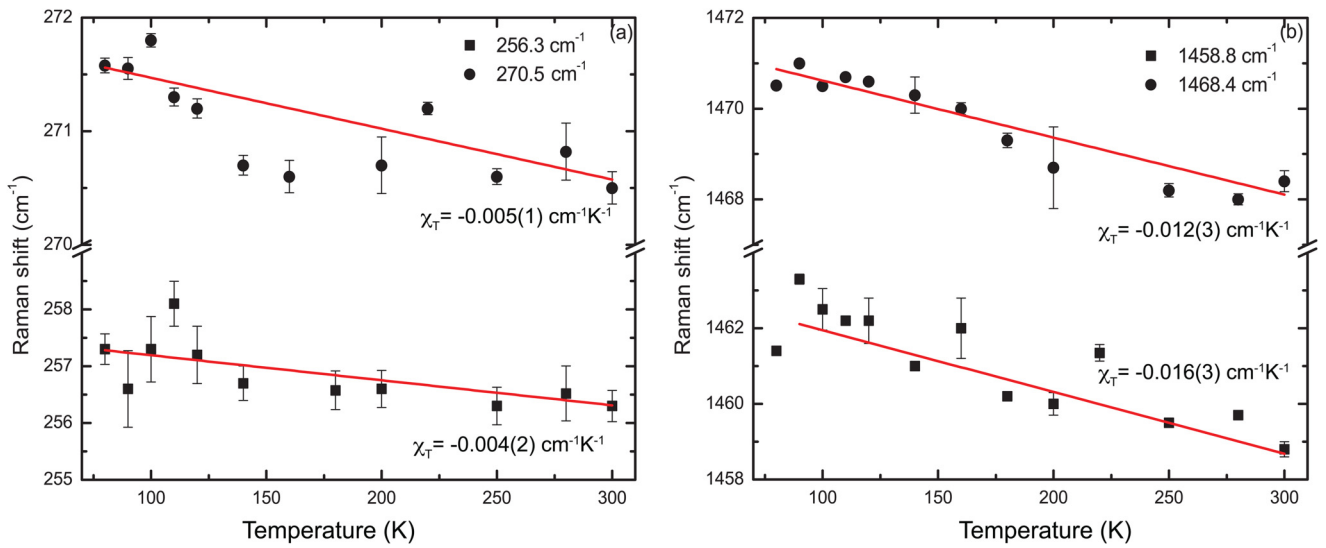

FIG. 3. Temperature dependent Raman shifts observed at (a) 256.3 cm^{-1} and 270.5 cm^{-1} and (b) 1458.8 cm^{-1} and 1468.4 cm^{-1} peaks.

TABLE I. Temperature dependent frequency coefficients (χ_T) and the frequency at absolute zero (ω_0) of various vibrational modes of $C_{60}O$.

Peak position (cm^{-1})	χ_T (cm^{-1} K^{-1})	ω_0 (cm^{-1})
256.3	−0.004(2)	257.6(3)
270.5	−0.005(1)	271.9(2)
1458.8	−0.016(3)	1463.6(5)
1468.4	−0.012(3)	1471.9(3)

shift. The laser power dependent Raman spectra of $C_{60}O$ were obtained at room temperature using 514.5 nm excitation and by varying the laser power between 0.1 mW and 0.5 mW. At 0.1 mW, $C_{60}O$ vibrational modes are found at 256.5(6) cm^{-1} and 270.7(2) cm^{-1} and their variation with laser power is plotted in Fig. 5. Upon increasing the laser power to 0.5 mW, 256.5 cm^{-1} peak shifts by −1.2(5) cm^{-1} and 270.7 cm^{-1} peak shifts by −0.7(1) cm^{-1}. The linear power coefficients (χ_L) are found to be −2.9(6) cm^{-1}/mW and −2.8(9) cm^{-1}/mW for 256.5 cm^{-1} and 270.7 cm^{-1} peaks, respectively. With an increase in the laser power, the local temperature of the fullerene thin films increases which leads to redshift in their Raman frequencies.

The steady state thermal conductivity of nanoscale systems is reportedly small and remains nearly independent of the carrier frequencies.[38] However, previous reports on molecular dynamics simulations of C_{60} crystals have shown that the heat conduction is mostly contributed by the low frequency phonons (< 100 cm^{-1}) which arise due to intermolecular interactions.[4,9] Due to experimental constraints, the thermal variation in the Raman frequencies greater than 200 cm^{-1} is considered for the thermal conductivity measurements in $C_{60}O$ films. For homogeneous and semi-infinite sample (sample thickness > the laser diameter), the steady state thermal conductivity, κ, is given by[39,40]

$$\kappa = \frac{L}{\sqrt{\pi} a \Delta T}, \tag{2}$$

where a Gaussian profiled laser beam having a as $1/e^2$ width is used to generate the heat flux, ΔT is the rise in the local temperature due to laser heating, and L is the laser power. To examine the spectral contributions to the heat conduction, κ is evaluated for both low and high frequencies at 256.5 cm^{-1} and 488.9 cm^{-1}. At 0.15 mW, ΔT are found to be 35 K and 30 K, and κ are found to be 0.7(2) W m^{-1} K^{-1} and 0.8(3) W m^{-1} K^{-1}, respectively, for 256.5 cm^{-1} and 488.9 cm^{-1} peaks. This shows that the thermal conduction is nearly independent of the carrier frequencies. In endohedral fullerenes $M@C_{82}$, thermal conductivities are reportedly larger than that of C_{60} and $C_{60}O$.[16] This could be attributed to the Raman frequencies considered for the evaluation of the thermal conductivities of the endohedral fullerenes which are smaller (<200 cm^{-1}) than that of $C_{60}O$.

Unlike graphene, fullerene molecules offer high Seebeck coefficients and low thermal conductivities which collectively enhance the figure of merits and thermopower of fullerene based thermoelectric materials.[2,41] The Seebeck coefficient and electrical conductance of C_{60}, C_{82}, and $M@C_{82}$ molecules have been previously reported and are utilized for the comparison of their figure of merits.[15,42] As the thermal conductivity of C_{60} is much smaller than that of $M@C_{82}$, it is better suited and thus is applied for the thermoelectric applications.[3,7,16] Our findings suggest that $C_{60}O$, whose thermal conductivity is at par with C_{60} and nearly 50 times smaller than that of $M@C_{82}$, may also find suitable applications in thermoelectric devices.

C. Pressure dependent Raman analysis

Figure 6 shows pressure dependent Raman spectra of $C_{60}O$ up to 5.5 GPa. The frequency range from 1250 cm^{-1} to 1400 cm^{-1} is overshadowed by a strong 1332 cm^{-1} peak of diamond in the pressure cell. Due to this, the spectra were taken in two separate regions (i) 200-600 cm^{-1} and (ii) 1400-1600 cm^{-1}. At ambient pressure, due to the presence of oxygen, the degenerate Raman modes are observed at

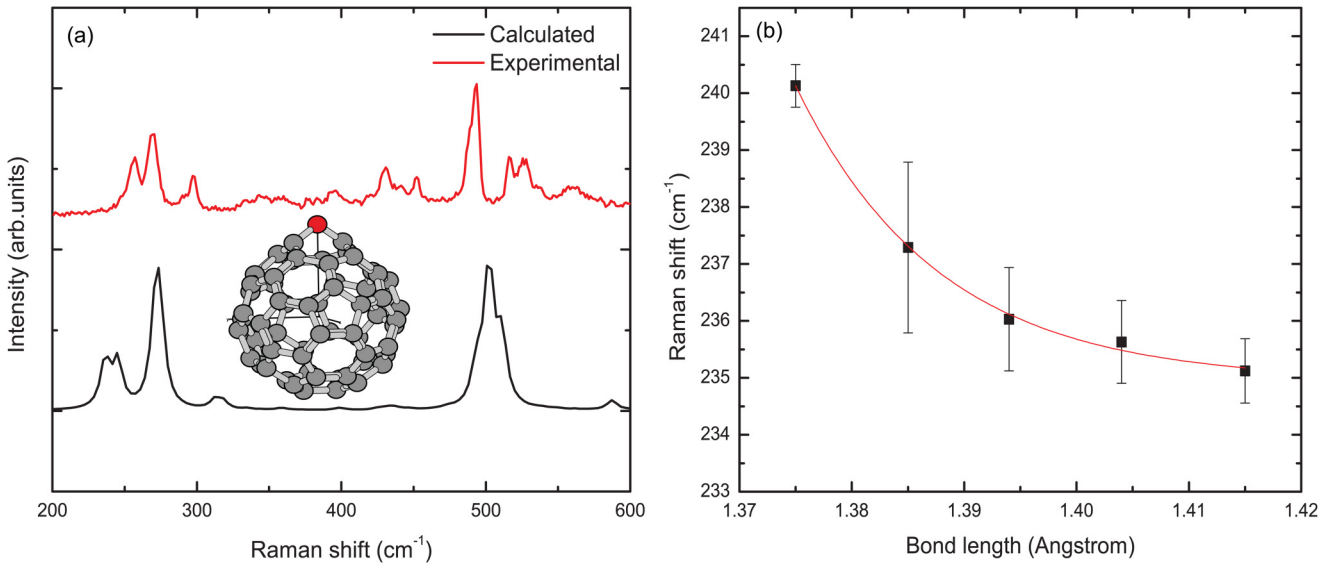

FIG. 4. (a) Experimental and calculated Raman spectra of $C_{60}O$ in the region 200-600 cm^{-1}. (b) Raman shift in the 235.7 cm^{-1} peak as a function of C–O bond length.

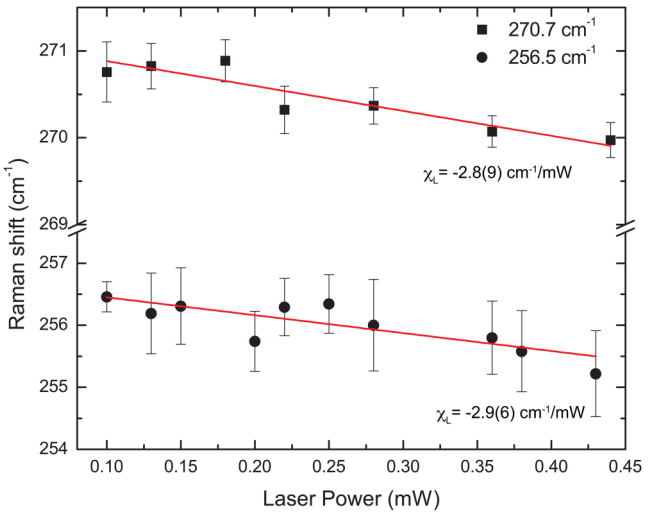

FIG. 5. Laser power dependent Raman shift in 256.5 cm^{-1} and 270.7 cm^{-1} peaks of $C_{60}O$.

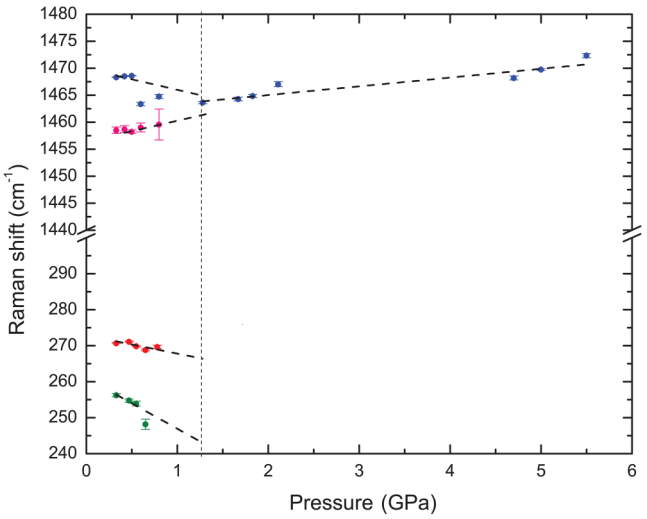

FIG. 7. Pressure dependent Raman shift observed for degenerate H_g mode (256.3 cm^{-1} and 270.7 cm^{-1}) and degenerate A_g mode (1458.5 cm^{-1} and 1468.3 cm^{-1}) of $C_{60}O$. A dotted vertical line at 1.2 GPa is used to demarcate between Phase I and Phase II of $C_{60}O$.

256.3(4) cm^{-1} and 270.7(2) cm^{-1} and at 1458.5(6) cm^{-1} and 1468.3(1) cm^{-1}. The observed shift in these Raman peaks with the applied pressure is shown in Fig. 7. Both 256.3 cm^{-1} and 270.7 cm^{-1} peaks redshift upon increasing the pressure up to 0.8 GPa. Above 1 GPa, both peaks disappear. The peak at 1458.5 cm^{-1} shifts to higher frequencies, whereas 1468.3 cm^{-1} peak redshifts upon increasing the pressure to 1.2 GPa. Above 1.2 GPa, two peaks appear as one at 1463.8(2) cm^{-1} which shifts linearly to higher frequencies with pressure up to 5.5 GPa. By releasing the pressure, the reappearance of 1458.5 cm^{-1} and 1468.3 cm^{-1} peaks was seen, whereas no notable modes were observed in the low frequency region.

The linear pressure coefficient ($d\omega/dp$) for each mode is evaluated and is presented in Table II. At 0.8 GPa, the peaks at 256.3 cm^{-1} and 270.7 cm^{-1} redshift by 8 cm^{-1} and 1 cm^{-1}, respectively, as compared to that at atmospheric pressure. Unlike graphite where the pressure below 1.2 GPa has negligible effects on the C–C bonds, we conclude that the observed redshifts in C–C and C–O modes with pressure are due to reduced inter-molecular spacing and subsequent compression of the $C_{60}O$ cluster.[43,44] Compressing the molecular cluster not only reduces the lattice parameter but also constrains the rotational motion of the molecules. The change in $d\omega/dp$ of 1468.3 cm^{-1} peak at 1.2 GPa is attributed to the C_{60} orientational phase transition[22] where the applied pressure increases the interaction between the neighboring molecules leading to the formation of inter-molecular bonds and thus their polymerization.[45] From the obtained results, we infer that above 1.2 GPa pressure, polymerization of $C_{60}O$ occurs.

The covalent bonds between neighboring fullerene cages may modify the interaction potential and can result in the

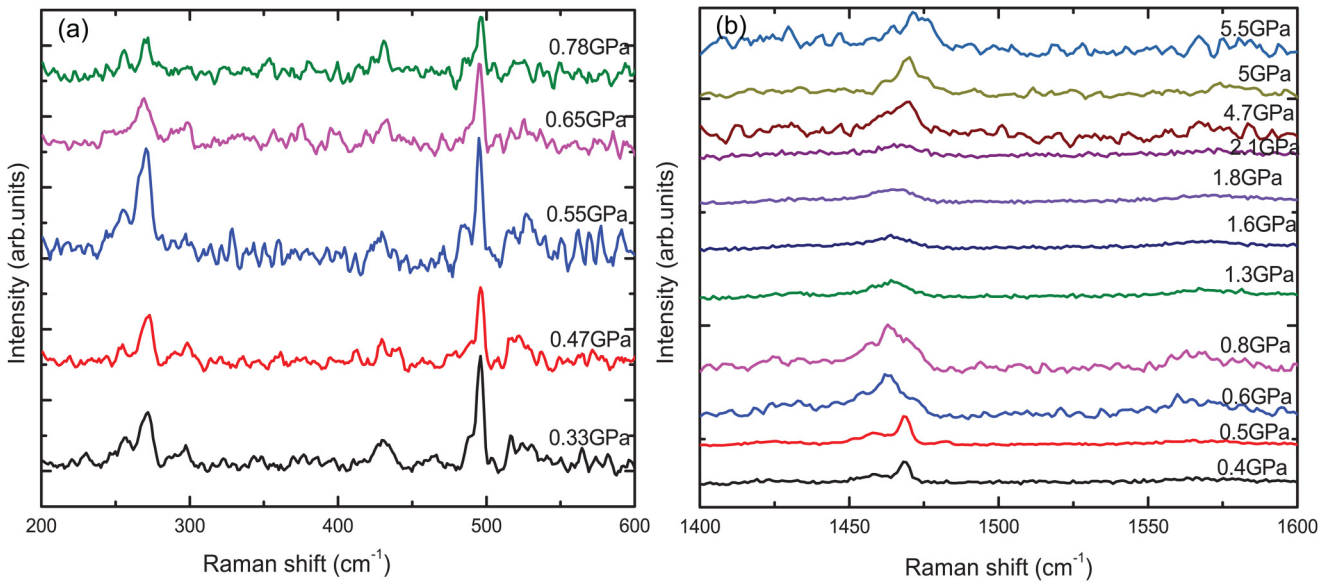

FIG. 6. Pressure dependent Raman spectra of $C_{60}O$ in the frequency range (a) 200-600 cm^{-1} and (b) 1400-1600 cm^{-1}.

TABLE II. Pressure dependent frequency coefficients ($d\omega/dp$) of various vibrational modes of $C_{60}O$.

Peak position (cm^{-1} at 1 atm)	$d\omega/dp$ (Phase I) (cm^{-1} GPa^{-1})	$d\omega/dp$ (Phase II) (cm^{-1} GPa^{-1})
256.3	−14(7)	...
270.7	−5(3)	...
1458.5	4(2)	...
1468.3	−4(2)	1.6(2)

increase in Debye temperature and heat transport.[46] A similar increase in the thermal conductivity of compressed C_{60} clusters is reported for the pressure above 0.3 GPa.[47] An effective compression of these cages inside the carbon nanotube peapod structures has also presented change in their conductivities.[48] Unlike the bulk samples, the studies on C_{60} dimer junctions have shown that their thermal conductivities are nearly 20 times smaller than that of the monomer.[42,49] Despite having larger thermopowers and Seebeck coefficients, the dimers and other higher clusters show smaller figure of merits as compared to the single C_{60} molecule.[49,50] This has been attributed to both electronic as well as phononic contributions to the thermal conductivities of the dimers.[49] As the applied pressure initiates the polymerization of C_{60}, we propose that the pressure induced structural changes in $C_{60}O$ molecules as well as the clusters may tune the carrier's contribution to the thermal conductance and may act as a mean to moderate their thermoelectric efficiency.

IV. CONCLUSIONS

In summary, we have synthesized $C_{60}O$ by the photolysis method. The temperature, pressure, and laser power dependent Raman spectra of $C_{60}O$ thin films have been examined. The temperature dependent shift in the phonon modes shows contraction in the fullerene cage and C–O bond length at low temperatures. Thermal effects on the Raman frequencies are utilised for evaluating the thermal conductivity of $C_{60}O$ thin films and is found to be 0.7(2) $W\,m^{-1}\,K^{-1}$ which is marginally greater than that of C_{60}. Thanks to their low thermal conductivities, which are the prerequisites for higher figure of merits, both C_{60} as well as its oxide version appear as potential candidates for the thermoelectric applications.

In addition, a pressure dependent Raman study is also performed on $C_{60}O$ at room temperature. Redshift in the low frequency Raman modes is ascribed to the compression of the cluster and thus the constrained rotational motion of the molecules. Polymerization of $C_{60}O$ is also observed at high pressures and is found to be reversible with the release of pressure. Pressure induced polymerization in $C_{60}O$ films may modulate its thermal properties and the conductivity which may decide its thermal efficiency for future applications.

ACKNOWLEDGMENTS

A.T. and T.M. thankfully acknowledge UGC-DAE-CSR Indore for providing financial support and the lab facilities. The authors are grateful to Dr. D. Rai, Sikkim University, for the useful discussion on DFT. The authors are also thankful to Dr. V. Sathe, UGC-DAE-CSR Indore, for help during the experiments.

[1]M. S. Dresselhaus, G. Chen, M. Y. Tang, R. G. Yang, H. Lee, D. Z. Wang, Z. F. Ren, J.-P. Fleurial, and P. Gogna, "New directions for low-dimensional thermoelectric materials," Adv. Mater. **19**(8), 1043–1053 (2007).
[2]K. Zhang, Y. Zhang, and S. R. Wang, "Enhancing thermoelectric properties of organic composites through hierarchical nanostructures," Sci. Rep. **3**, 3448 (2013).
[3]C. Kim, D. S. Suh, K. H. P. Kim, Y. S. Kang, T. Y. Lee, Y. Khang, and D. G. Cahill, "Fullerene thermal insulation for phase change memory," Appl. Phys. Lett. **92**, 013109 (2008).
[4]L. Chen, X. Wang, and S. Kumar, "Thermal transport in fullerene derivatives using molecular dynamics simulations," Sci. Rep. **5**, 12763 (2015).
[5]J. Vavro, M. C. Llaguno, B. C. Satishkumar, D. E. Luzzi, and J. E. Fischer, "Electrical and thermal properties of C_{60}-filled single-wall carbon nanotubes," Appl. Phys. Lett. **80**(8), 1450–1452 (2002).
[6]N. H. Tea, R. C. Yu, M. B. Salamon, D. C. Lorents, R. Malhotra, and R. S. Ruoff, "Thermal conductivity of C_{60} and C_{70} crystals," Appl. Phys. A **56**, 219–225 (1993).
[7]X. Wang, C. D. Liman, N. D. Treat, M. L. Chabinyc, and D. G. Cahill, "Ultralow thermal conductivity of fullerene derivatives," Phys. Rev. B **88**(7), 075310 (2013).
[8]J. C. Duda, P. E. Hopkins, Y. Shen, and M. C. Gupta, "Exceptionally low thermal conductivities of films of the fullerene derivative PCBM," Phys. Rev. Lett. **110**(1), 015902 (2013).
[9]A. Giri and P. E. Hopkins, "Spectral contributions to the thermal conductivity of C_{60} and the fullerene derivative PCBM," J. Phys. Chem. Lett. **8**(10), 2153–2157 (2017).
[10]R. Taylor, J. P. Parsons, A. G. Avent, S. P. Rannard, T. J. Dennis, J. P. Hare, H. W. Kroto, and D. R. M. Walton, "Degradation of C_{60} by light," Nature **351**, 277 (1991).
[11]L. Juha, J. Krása, L. Láska, V. Hamplová, L. Soukup, P. Engst, and P. Kubát, "Fast degradation of fullerenes by ultraviolet laser radiation," Appl. Phys. B **57**(1), 83–84 (1993).
[12]K. M. Creegan, W. K. Robbins, J. L. Robbins, J. M. Millar, R. D. Sherwood, P. J. Tindall, D. M. Cox, A. B. Smith, III, J. P. McCauley, D. R. Jones, and R. T. Gallagher, "Synthesis and characterization of $C_{60}O$, the first fullerene epoxide," J. Am. Chem. Soc. **144**, 1103 (1992).
[13]B. C. Wang, L. Chen, and Y. M. Chou, "Theoretical studies of C_{60}/C_{70} fullerene derivatives: $C_{60}O$ and $C_{70}O$," J. Mol. Struct. **422**(1), 153–158 (1998).
[14]R. Dattani, K. F. Gibson, S. Few, A. J. Borg, P. A. DiMaggio, J. Nelson, S. G. Kazarian, and J. T. Cabral, "Fullerene oxidation and clustering in solution induced by light," J. Colloid Interface Sci. **446**, 24–30 (2015).
[15]S. K. Lee, M. Buerkle, R. Yamada, Y. Asai, and H. Tada, "Thermoelectricity at the molecular scale: a large Seebeck effect in endohedral metallofullerenes," Nanoscale **7**(48), 20497–20502 (2015).
[16]T. Mondal, A. Tripathi, J. Zhang, T. Shripathi, H. Shinohara, and A. Tiwari, "Thermal conductivity of M@C_{82} [M= Dy, Gd] thin films," J. Phys. Chem. C **121**(6), 3642–3647 (2017).
[17]Y. Gao and B. Xu, "Probing thermal conductivity of fullerene C_{60} hosting a single water molecule," J. Phys. Chem. C **119**(35), 20466–20473 (2015).
[18]Y. Murakami and H. Suematsu, "Magnetism of C_{60} induced by photo-assisted oxidation," Pure Appl. Chem. **68**, 1463–1467 (1996).
[19]R. Liu and M. V. Klein, "Raman study of vibrational properties in solid C_{60}," Phys. Rev. B **45**, 11437 (1992).
[20]M. Krause, L. Dunsch, G. Seifert, P. W. Fowler, A. Gromov, W. Kratschmer, R. Gutierez, D. Porezag, and T. Frauenheim, "Vibrational signatures of fullerene oxides," J. Chem. Soc., Faraday Trans. **94**, 2287–2294 (1998).
[21]B. Chase, N. Herron, and E. Holler, "Vibrational spectroscopy of fullerenes (C_{60} and C_{70}). Temperature dependant studies," J. Phys. Chem. **96**(11), 4262–4266 (1992).
[22]S. J. Jeon, D. Kim, S. K. Kim, and I. C. Jeon, "High-pressure Raman study of fullerite C_{60}," J. Raman Spectrosc. **23**(5), 311–313 (1992).
[23]A. M. Rao, P. Zhou, K.-A. Wang, G. T. Hager, J. M. Holden, Y. Wang, W.-T. Lee, X.-X. Bi, P. C. Eklund, D. S. Cornett *et al.*, "Photoinduced polymerization of solid C_{60} films," Science **259**, 955–957 (1993).
[24]D. Heymann and L. P. F. Chibante, "Photo-transformations of C_{60}, C_{70}, $C_{60}O$, and $C_{60}O_2$," Chem. Phys. Lett. **207**(4-6), 339–342 (1993).

[25]R. J. Angel, M. Bujak, J. Zhao, G. D. Gatta, and S. D. Jacobsen, "Effective hydrostatic limits of pressure media for high-pressure crystallographic studies," J. Appl. Crystallogr. **40**(1), 26–32 (2007).
[26]S. Klotz, J. C. Chervin, P. Munsch, and G. Le Marchand, "Hydrostatic limits of 11 pressure transmitting media," J. Phys. D: Appl. Phys. **42**(7), 075413 (2009).
[27]A. Jayaraman, "Diamond anvil cell and high-pressure physical investigations," Rev. Mod. Phys. **55**(1), 65 (1983).
[28]D. S. Bethune, G. Meijer, W. C. Tang, and H. J. Rosen, "The vibrational Raman spectra of purified solid films of C_{60} and C_{70}," Chem. Phys. Lett. **174**(3-4), 219–222 (1990).
[29]D. S. Bethune, G. Meijer, W. C. Tang, H. J. Rosen, W. G. Golden, H. Seki, C. A. Brown, and M. S. de Vries, "Vibrational Raman and infrared spectra of chromatographically separated C_{60} and C_{70} fullerene clusters," Chem. Phys. Lett. **179**(1-2), 181–186 (1991).
[30]S. Lebedkin, A. Gromov, S. Giesa, R. Gleiter, B. Renker, H. Rietschel, and W. Krätschmer, "Raman scattering study of C_{120}, a C_{60} dimer," Chem. Phys. Lett. **285**(3), 210–215 (1998).
[31]I. Calizo, A. A. Balandin, W. Bao, F. Miao, and C. N. Lau, "Temperature dependence of the Raman spectra of graphene and graphene multilayers," Nano Lett. **7**, 2645–2649 (2007).
[32]A. V. Talyzin, A. Dzwilewski, and T. Wågberg, "Temperature dependence of C_{60} Raman spectra up to 840 K," Solid State Commun. **140**(3-4), 178–181 (2006).
[33]M. J. Frisch, G. W. Trucks, H. B. Schlegel, G. E. Scuseria, M. A. Robb, J. R. Cheeseman, G. Scalmani, V. Barone, B. Mennucci, G. A. Petersson *et al.*, Gaussian 09, Revision A.02, Gaussian, Inc., Wallingford, CT, 2009.
[34]K. Raghavachari, "Structure of $C_{60}O$: unexpected ground state geometry," Chem. Phys. Lett. **195**(2-3), 221–224 (1992).
[35]M. Menon and K. R. Subbaswamy, "Optimized structures of $C_{60}O$ and $C_{60}O_2$ calculated by a damped molecular dynamics optimization scheme," Chem. Phys. Lett. **201**(1-4), 321–325 (1993).
[36]F. Gugenberger, R. Heid, C. Meingast, P. Adelmann, M. Braun, H. Wühl, M. Haluska, and H. Kuzmany, "Glass transition in single-crystal C_{60} studied by high-resolution dilatometry," Phys. Rev. Lett. **69**(26), 3774 (1992).
[37]A. T. Pugachev, N. P. Churakova, N. I. Gorbenko, Kh. Saadli, and E. S. Syrkin, "Thermal expansion of thin C_{60} films," J. Exp. Theor. Phys. **87**(5), 1014–1018 (1998).
[38]F. X. Alvarez and D. Jou, "Size and frequency dependence of effective thermal conductivity in nanosystems," J. Appl. Phys. **103**(9), 094321 (2008).
[39]B. Stoib, S. Filser, J. Stötzel, A. Greppmair, N. Petermann, H. Wiggers, G. Schierning, M. Stutzmann, and M. S. Brandt, "Spatially resolved determination of thermal conductivity by Raman spectroscopy," Semicond. Sci. Tech. **29**(12), 124005 (2014).
[40]J. L. Braun, C. J. Szwejkowski, A. Giri, and P. E. Hopkins, "On the steady-state temperature rise during laser heating of multilayer thin films in optical pump–probe techniques," J. Heat Transfer **140**(5), 052801 (2018).
[41]J. H. Seol, I. Jo, A. L. Moore, L. Lindsay, Z. H. Aitken, M. T. Pettes, X. Li, Z. Yao, R. Huang, D. Broido, and N. Mingo, "Two-dimensional phonon transport in supported graphene," Science **328**(5975), 213–216 (2010).
[42]C. Evangeli, K. Gillemot, E. Leary, M. T. Gonzalez, G. Rubio-Bollinger, C. J. Lambert, and N. Agraït, "Engineering the thermopower of C_{60} molecular junctions," Nano Lett. **13**(5), 2141–2145 (2013).
[43]R. Clarke and C. Uher, "High pressure properties of graphite and its intercalation compounds," Adv. Phys. **33**(5), 469–566 (1984).
[44]J. E. Fischer, P. A. Heiney, A. R. McGhie, W. J. Romanow, A. M. Denenstein, J. P. McCauley, and A. B. Smith, "Compressibility of solid C_{60}," Science **252**(5010), 1288–1290 (1991).
[45]B. Sundqvist, "The structures and properties of C_{60} under pressure," Phys. B: Cond. Mat. **265**(1-4), 208–213 (1999).
[46]A. Soldatov and O. Andersson, "Thermal conductivity of pressure polymerized C_{60}," Appl. Phys. A **64**(3), 227–229 (1997).
[47]O. Andersson, A. Soldatov, and B. Sundqvist, "Thermal conductivity of C_{60} at pressures up to 1 GPa and temperatures in the 50–300 K range," Phys. Rev. B **54**(5), 3093 (1996).
[48]T. Kodama, M. Ohnishi, W. Park, T. Shiga, J. Park, T. Shimada, H. Shinohara, J. Shiomi, and K. E. Goodson, "Modulation of thermal and thermoelectric transport in individual carbon nanotubes by fullerene encapsulation," Nat. Mater. **16**(9), 892 (2017).
[49]J. C. Klöckner, R. Siebler, J. C. Cuevas, and F. Pauly, "Thermal conductance and thermoelectric figure of merit of C_{60}-based single-molecule junctions: electrons, phonons, and photons," Phys. Rev. B **95**(24), 245404 (2017).
[50]N. Almutlaq, Q. Al-Galiby, S. Bailey, and C. J. Lambert, "Identification of a positive-Seebeck-coefficient exohedral fullerene," Nanoscale **8**(28), 13597–13602 (2016).